08

$Zn_xFe_{3-x}O_4$ ($0 \leq x \leq 1.0$) magnetic nanoparticles functionalized with polyacrylic acid (PAA)

© A.S. Kamzin,[1] G. Caliskan,[2] N. Dogan,[2] A. Bingolbali,[3] V.G. Semenov,[4] I.V. Buryanenko[5]

[1] Ioffe Institute,
194021 St. Petersburg, Russia
[2] Department of Physics, Gebze Technical University,
41400 Kocaeli, Turkey
[3] Department of Bioengineering, Yıldız Technical University,
34220 Istanbul, Turkey
[4] St. Petersburg State University,
199034 St. Petersburg, Russia
[5] St. Petersburg State University, St. Petersburg,
195251 St. Petersburg, Russia
e-mail: ASKam@mail.ioffe.ru

Received June 9, 2022
Revised July 24, 2022
Accepted August 13, 2022

Studies of the properties of $Zn_xFe_{3-x}O_4$ ($x = 0$, 0.25, 0.5, 0.75, 1.0) magnetic nanoparticles synthesized by a modified hydrothermal method are presented in comparison with the properties of the same nanoparticles stabilized with polyacrylic acid $Zn_xFe_{3-x}O_4$@PAA. The structure, size, morphology, and magnetic properties of the samples were studied by X-ray diffraction (XRD), Fourier transform infrared spectroscopy (FT IR), physical properties measurements (PPMS), and Mossbauer spectroscopy. The synthesized nanoparticles are single-phase, without additional impurities, have a narrow size distribution and are in the superparamagnetic phase. From the (XRD) measurements, it was found that with an increase in the Zn content from $x = 0$ to $x = 1.0$, the sizes of the nanoparticles were increasing from 17 to 33 nm. Analysis of the Mossbauer spectroscopy data showed that when doped with Zn ions from $x = 0$ to x=1.0, the sizes of the nanoparticles were decreasing from 15 nm to 5 nm. The results of the Mossbauer studies showed that both $Zn_xFe_{3-x}O_4$ and $Zn_xFe_{3-x}O_4$@PAA has a core/shell type structure in which the core is magnetically ordered, whereas the shell does not have magnetic ordering.

Mossbauer studies indicate that the coating of citric acid particles leads to their isolation from each other, reducing or eliminating interactions between particles, reducing the thickness of the paramagnetic shell, and thereby increasing the diameter of the core, which is in a magnetically ordered state.

Keywords: ferrite-spinel nanoparticles, hydrothermal synthesis, polyacrylic acid functionalization, Mossbauer spectroscopy, properties, crystal and magnetic structure.

DOI: 10.21883/TP.2022.12.55201.152-22

Introduction

Ferromagnetic fluid, ferrofluid (FMF) (from the Latin ferrum — iron) or magnetic fluid (MF), is a stable colloidal solution consisting of magnetic nanoparticles (MNP) suspended in a non-magnetic fluid [1]. Investigations of MF properties, development of new methods of synthesis and areas of their practical use were started from the middle 60s of the 20th century after the appearance of papers [2,3]. As a result, it was shown that the uniqueness of the MF lies in the combination of the base liquid fluidity and the ability of MNPs to interact with the magnetic field [4]. It was found that MFs are extremely promising materials for practical applications, such as magnetic fluid seals, magnetic lubricants, visualization systems for the structure of constant magnetic fields and the domain structure of magnetics, magnetically controlled light filters, hydromechanical transducers, sound emitters and spintronic devices, etc. [5–7].

The most relevant application of MF is in biomedicine, for the delivery of drugs or diagnostic agents to a diseased organ [8,9]. The method of magnetic hyperthermic treatment of malignant tumors by introducing MF into tumors and subsequent heating of MNPs by an alternating magnetic field is being intensively developed, which leads to local destruction of cancer cells [10].

The properties of MF are determined by the combination of characteristics of its constituent components (magnetic phase, dispersion medium, and stabilizer), which changing ensures MF parameters control. Mainly, MFs are determined by the MNP properties, which depend on the composition, magnetic properties, MNP structure, particles size, and distribution by sizes. The type, thickness, and structure of the particle functionalization (coating) material

are also important, because the coating is a unique tool for significant change of the particle surface structure due to bonds with atoms on the MNP surface. All this is the subject of extensive studies [7,11–13]. The MF stability is ensured by the MNP functionalization with a surfactant or ionic materials that form a protective shell around the particles and prevent conglomeration. Surfactants prevent particles from sticking together and forming heavy clusters that are not held in suspension by Brownian motion. In the case of an ideal MF, the MNP settling does not occur in a gravitational and even in a very strong magnetic field. Surfactant molecules have a polar „head" and a non-polar „tail" (or vice versa); one of the ends is adsorbed to the particle, while the other is attached to the molecules of the carrier liquid, forming, respectively, a regular or reverse micelle around the particle. As a result, spatial effects prevent particles from sticking together. Although surfactants are useful for extending the settling time of particles in fluid, they prove to be detrimental to its magnetic properties (in particular, to the magnetic saturation of the MF). The surface layer of surfactant (or other coatings) can reduce the packing density of ferromagnetic particles in the activated state of MF, and also change the magnetic characteristics of the particles. In this regard, it is necessary to study the coating effect on MNP properties.

For the purpose of using in MF the magnetite particles Fe_3O_4 doped with divalent metal ions ($M_xFe_{3-x}O_4$, where M = Ni, Mn, Zn) are widely studied because such metals introduction leads to an improvement of the magnetic characteristics of the material. For the MNP synthesis various methods of magnetic particles obtaining are used, such as coprecipitation, hydrothermal, microwave combustion, sol-gel spontaneous combustion, spray pyrolysis, etc. [14–20]. The method of synthesis also influences structural properties, namely size, morphology, surface condition and chemical homogeneity. However, despite the large number of works on the MNPs synthesis for MFs, published data on the different coatings effect on the magnetic properties of nanoparticles are far from sufficient. Therefore, comprehensive studies of the properties and magnetic structure dependence on the particles functionalization are of great interest.

This paper presents the results of studies of MNP, i. e. Zn-substituted magnetite ($Zn_xFe_{3-x}O_4$) depending on the number of ions Zn ($x = 0$, 0.25, 0.5, 0.75, 1.0), and of studies the effect of functionalization (coating) with polyacrylic acid (PAA) on the properties of particles $Zn_xFe_{3-x}O_4$@PAA. Zn^{2+} ions for magnetite doping were chosen due to the unusual properties of $Zn_xFe_{3-x}O_4$ ferrites, which attract researchers to study them for various applications [21,22]. The introduction of even a small amount of Zn into magnetite can significantly increase the saturation magnetization of MNP $Zn_xFe_{3-x}O_4$ [23,24]. Ferrimagnetic properties can be observed in MNPs of $Zn_xFe_{3-x}O_4$ zinc ferrite at temperatures above the magnetic ordering point.

PAA was used as a stabilizing material for the following reasons. PAA compared to other acids, such as citric acid, provides a high density of reactive functional groups, excellent stability, and prevents the adsorption of blood plasma proteins [25]. The absence of coercive forces and retained magnetization of MNPs functionalized with PAA prevents magnetic interaction between particles, and the formation of conglomerates and small clusters, which is important for various MF applications. PAA-coated MNPs are also promising for biomedical applications, which is determined by their biocompatibility, lack of cytotoxicity, and ability to stay in a living organism for a reasonable time [26]. PAA functionalization provides strong adsorption (resistance to dilution) and electrosteric repulsion between MNPs, overcoming Van der Waal's forces and forces of magnetic dipole-dipole attraction, which significantly increases the colloidal stability of the MF. All this makes it necessary to study the PAA effect on the properties of $Zn_xFe_{3-x}O_4$ MNPs in order to create highly stabilized monodisperse materials required for various applications.

1. Materials and research techniques

1.1. Synthesis and PAA functionalization of MNP $Zn_xFe_{3-x}O_4$ ($x = 0, 0.25, 0.5, 0.75, 1.0$)

For the synthesis of MNPs $Zn_xFe_{3-x}O_4$ ($x = 0$, 0.25, 0.5, 0.75, 1.0) iron chloride tetrahydrate ($FeCl_2 \bullet 4H_2O$), iron chloride hexahydrate ($FeCl_3 \bullet 6H_2O$), zinc chloride ($ZnCl_2$) and ammonium hydroxide (NH_4OH, 25% ammonia) were used from Sigma Aldrich with purity of 99%. To functionalize (surface coating) MNPs $Zn_xFe_{3-x}O_4$ and obtain $Zn_xFe_{3-x}O_4$@PAA particles PAA of 99.9% purity (Sigma Aldrich) was used.

Magnetic nanoparticles $Zn_xFe_{3-x}O_4$ ($x = 0$, 0.25, 0.5, 0.75, 1.0) were synthesized by the hydrothermal method, first proposed in 1845 and being a simple, cost-effective and environmentally friendly method [27,28]. For the synthesis of $Zn_xFe_{3-x}O_4$ nanoparticles with various amounts of Zn ($x = 0$, 0.25, 0.5, 0.75, 1.0) salts Fe^{3+} and Zn^{2+} in amounts of $(3-x)$ and (x) respectively were mixed in 40 ml of distilled water. The resulting mixture was mechanically stirred at room temperature at 500 rpm for 2 min in a nitrogen atmosphere, after which 5 ml of 25% aqueous solution of NH_4OH was added dropwise. The solution was sealed, placed in an autoclave, and kept at 180°C for 12 h. The autoclave was cooled naturally. The precipitate was washed three times with distilled water, and separation with magnet MNPs $Zn_xFe_{3-x}O_4$ MNPs were obtained, which were used to study the properties.

To functionalize by PAA the synthesized $Zn_xFe_{3-x}O_4$ particles were mixed with 50 ml of deionized water and 3 mmol of PAA and stirred in the ultrasonic bath at 65°C. Then, 1 ml of the aqueous solution of NH_4OH was added to the mixture by droplets and mechanically stirred for 30 min in nitrogen atmosphere. The final black products were washed with distilled water, dried at 60°C for 2 h,

and functionalized MNPs $Zn_xFe_{3-x}O_4$@PAA were used for studies.

1.2. Methods for studying MNPs $Zn_xFe_{3-x}O_4$ and $Zn_xFe_{3-x}O_4$@PAA ($x = 0, 0.25, 0.5, 0.75, 1.0$)

The interaction between PAA and zinc-doped iron oxide nanoparticles was studied using infrared spectroscopy with Fourier transform Perkin Elmer L160000R in the region from 4000 to 500 cm^{-1}. X-ray diffraction analysis was carried out using a Rigaku X-ray 2200 diffractometer with a wavelength of $\lambda = 0.154$ nm of CuK_α-radiation in the range of diffraction angles 20–90° (2θ) with a scan step of 0.02°. The morphology (shape), as well as the presence of agglomeration of the synthesized particles, was studied using scanning electron microscopy (SEM) using a JEOL 6700 electron microscope in combination with energy dispersive X-ray spectroscopy (EDX). EDX was used to analyze the elemental composition of the samples. Saturation magnetization (Ms), coercive field (Hc), and remained magnetization (Mr) were measured using the Quantum Design Model 6000 Physical Property Measurement System (PPMS).

Mossbauer spectroscopy was used to study the phase composition, magnetic interactions, magnetic relaxation phenomena, and the structure of synthesized particles. Mossbauer spectra of MNPs $Zn_xFe_{3-x}O_4$ and $Zn_xFe_{3-x}O_4$@PAA with coating were registered at 300 K in the geometry of gamma-quanta transmission through the sample. The electromagnetic drive, on which the ^{57}Co(Rh) source of gamma-radiation was attached, uses a triangular rate shape. The rate scale was calibrated by a α-Fe foil of the thickness of 6 μm at the room temperature. The analysis of the experimental MS of MNPs $Zn_xFe_{3-x}O_4$ was carried out using a special program [29] by restoring the probability functions of the distribution of effective magnetic fields $\{P(H_{\text{eff}})\}$. The hyperfine structure was modeled by the least squares method using Zeeman sextets and quadrupole doublets consisting of lines of the Lorentzian form [29]. Using the positions of the spectral lines on the rate scale, the hyperfine interaction (HFI) parameters are calculated: The isomer shift values are given relative to α-Fe at 300 K.

2. Results of IR Fourier-analysis (FT IR) of MNPs $Zn_xFe_{3-x}O_4$@PAA ($x = 0, 0.25, 0.5, 0.75, 1.0$)

The infrared spectra of the particles are shown in Fig. 1, where at 746 cm^{-1} the characteristic bands of Fe–O and Zn–O are observed in the tetrahedral and octahedral modes [30]. Intensive absorption peaks at 1390 and 1539 cm^{-1} are formed by the carboxyl group (COO–) of PAA, which means that the surface of the nanoparticles is covered by the PAA [31] coating agent. Besides, the broad bands appearing at 3256 cm^{-1} can be attributed to

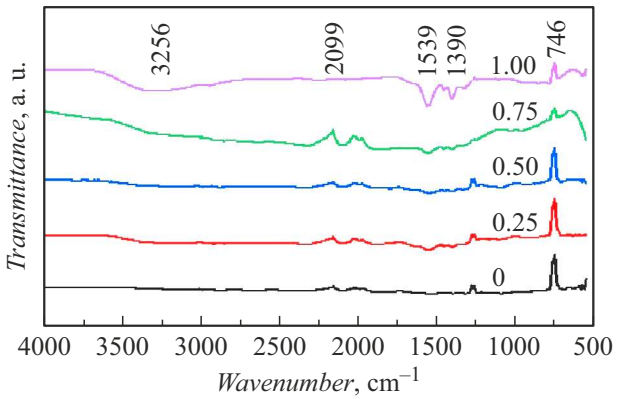

Figure 1. Infrared Fourier spectra of $Zn_xFe_{3-x}O_4$@PAA nanoparticles at $x = 0$, 0.25, 0.5, 0.75, 1 0.

stretching vibrations of the O–H bonds of adsorbed water. An asymmetric band of stretching oscillations C–H was observed at 2099 cm^{-1}. Thus, the IR Fourier-analysis of the lines confirms that the surfaces of zinc-doped iron oxide nanoparticles are coated with PAA.

3. X-ray diffraction patterns of $Zn_xFe_{3-x}O_4$@PAA MNPs ($x = 0, 0.25, 0.5, 0.75, 1.0$)

X-ray diffraction patterns (XDP) of MNPs $Zn_xFe_{3-x}O_4$@PAA (at $x = 0$, 0.25, 0.5, 0.75, 1.0) are shown in Fig. 2. The observed diffraction peaks (220), (311), (400), (422), (511) and (440) coincide with the lines of the cubic phase of spinel Fe_3O_4 (JCPDS file № 88-0315) [32]. The diffraction lines for the rest of the compositions correspond to the reflections for manganese ferrite indicated in the standard JCPDS card № 74-2403. This means that all synthesized particles are single-crystal, having a face-centered cubic structure

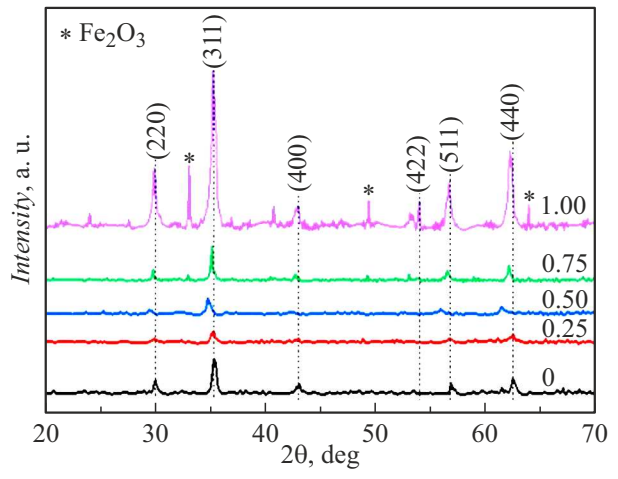

Figure 2. X-ray patterns of $Zn_xFe_{3-x}O_4$@PAA nanoparticles at $x = 0$, 0.25, 0.5, 0.75, 1.

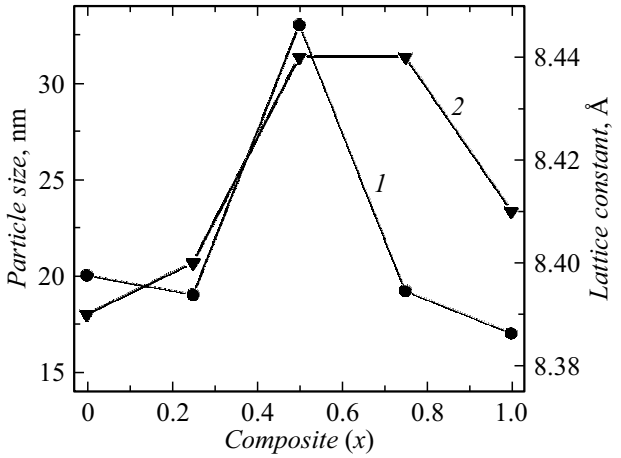

Figure 3. Average sizes of crystallites (*1*) and the lattice parameter (*2*) vs. value of substitution by Zn (x) ions for MNPs $Zn_xFe_{3-x}O_4$@PAA.

of inverse spinel [33,34]. Peak (311) at $2\theta = 35°$ is characteristic for single crystals of cubic spinel ferrite. Sufficiently wide diffraction lines observed in the X-ray diffraction pattern indicate that the samples consist of well-crystallized particles of small sizes, which is also confirmed by the Mossbauer study data described below. Note that the obtained XDPs are consistent with the literature, for example, [32–38]. All samples are monophasic, since there are no foreign phase lines (except for the $ZnFe_2O_4$@PAA sample). The X-ray diffraction pattern of $ZnFe_2O_4$@PAA composition shows a line (indicated by an asterisk) belonging to hematite, which is a secondary phase for this composition ($x = 1$).

The average sizes of crystallites were calculated using the Debye–Scherrer equation [33] and the line with index (311). For calculations, the instrumental broadening was subtracted from the linewidth. The results obtained are shown in Fig. 3, which shows that when magnetite is doped with Zn ions, the sizes of MNPs decrease from 20 nm ($x = 0$) to 17 nm ($x = 1.0$), except for particles $Zn_{0.5}Fe_{2.5}O_4$@PAA, whose dimensions are 33 nm.

The lattice parameters (a) of the samples were calculated using the equation

$$a = d_{hkl}\sqrt{h^2 + k^2 + l^2}, \qquad (1)$$

where h, k, l are the Miller indices and d_{hkl} is the distance between the planes. The average lattice constant for magnetite MNPs is $a = 8.39$ Å, which is close to the value for a macroscopic magnetite crystal (8.396 Å) [39]. Figure 3 shows that the lattice parameter increases with Zn concentration increasing from $x = 0$ to 0.5 and does not change up to $x = 0.75$. A further increasing of the amount of Zn doped to $x = 1.0$ leads to abrupt decreasing of the lattice parameter to a value slightly smaller than that observed at $x = 0.5$.

4. SEM and EDX results

The SEM photographs of the synthesized $Zn_xFe_{3-x}O_4$@PAA particles are shown in Fig. 4, they are used to determine the shape, size, and distribution of particles by sizes in the samples at different values of doping with Zn ions. Fig. 4 shows that the particles of Fe_3O_4@PAA sample have the largest average size. We should especially highlight the $Zn_{0.75}Fe_{2.25}O_4$@PAA sample, the analysis of photographs of which showed that with such doping with Zn ions the smallest particles distribution by sizes takes place, as well as minimal agglomeration. In the case of the $ZnFe_2O_4$@PAA sample, the particles have approximately spherical shape, the smallest dimensions, and insignificant agglomeration. Analysis of the EDX data showed a very good agreement between the Zn/Fe ratio in the samples under study and the specified amounts of components during synthesis.

Perhaps the use of SEM with better resolution or with high resolution would allow the particle structure to be established. However, even high-resolution electron microscopy often fails to distinguish between the core and shell due to the similarity of their phase-contrast image [40]. In such cases, the use of Mossbauer spectroscopy ^{57}Fe makes it possible to obtain unique information about the structural and magnetic properties of ferrite-spinels [40–42], as well as bimagnetic structures of the core–shell type [43–45]. This is due to the fact that Mossbauer spectroscopy can distinguish between different states of iron, since the isomer shift (IS) is sensitive to the oxidation degree of iron (Fe^{2+}, Fe^{3+} in spinels) and the quadrupole splitting (QS) is sensitive to different types of structural positions (octahedral and tetrahedral in spinels) and positions of neighboring ions. All this makes it possible to distinguish polymorphic modifications of Fe_2O_3 (magnetite from maghemite and hematite and others). Besides, using the Mossbauer effect, information about the magnetic structure can be extracted from the values of the effective magnetic fields (H_{eff}), because iron-containing materials in the superparamagnetic (unblocked) and ferromagnetic/antiferromagnetic (blocked) states have essentially different values of the effective fields. In addition, the particle size distribution is related to the full width at half-amplitude of the absorption line in the Mossbauer spectrum, as well as to the distributions of the Mossbauer spectroscopy parameters ^{57}Fe.

5. PPMS-measurement data

Curves of saturation magnetization (Ms) (M–H hysteresis loops), coercive field (Hc) and remained magnetization (Mr) obtained at room temperature using a Physical Property Measurement System (PPMS) are shown in Fig. 5.

The value of Ms-samples, as can be seen in Fig. 6, at $x = 0$ is 78 emu/g, which is slightly lower than the value for the macrocrystal Fe_3O_4 ($Ms \sim 82$ emu/g). With introducing Zn ($x = 0.25$), Ms value increases and reaches 86 emu/g. A

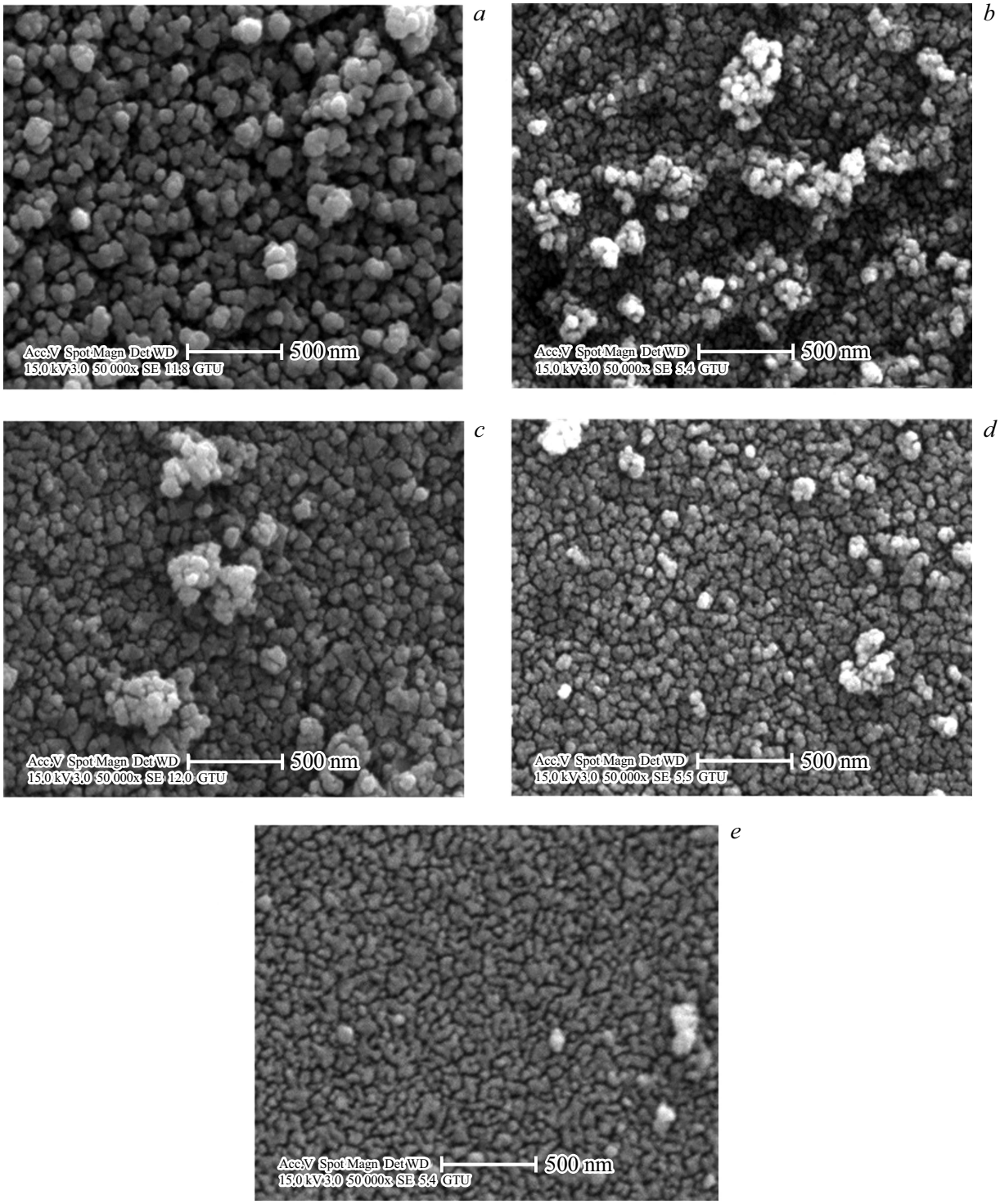

Figure 4. SEM photographs of $Zn_xFe_{3-x}O_4$@PAA particles. The Zn doping values are $x = 0$ (*a*), 0.25 (*b*), 0.5 (*c*), 0.75 (*d*) and 1.0 (*e*) respectively.

further increasing of Zn amount leads to value decreasing of Ms to 19 emu/g. The field of coecivity Hc is in the range 7.1−63.2 Oe. The ratios of remained magnetization values to Ms values (hysteresis loop squareness) calculated for MNPs $Zn_xFe_{3-x}O_4$@PAA MNPs are in the range of 0.003 −0, which indicates the superparamagnetic behavior of the particles. The values of the hysteresis loop squareness below 0.5 can be attributed to the effects of the disordered state of the magnetic moments of ions located in the surface layer of particles [47]. According to the values Ms and Hc, it can be stated that the synthesized MNPs $Zn_xFe_{3-x}O_4$ are in the superparamagnetic state (see [36] and references

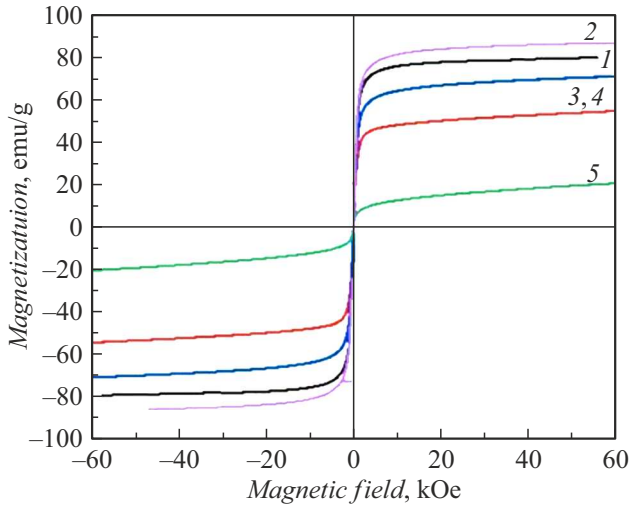

Figure 5. Magnetization (Ms) of MNPs $Zn_xFe_{3-x}O_4$@PAA vs. external magnetic field at $x = 0$, 0.25, 0.5, 0.75, 1 (labeled — *1, 2, 3, 4, 5* respectively).

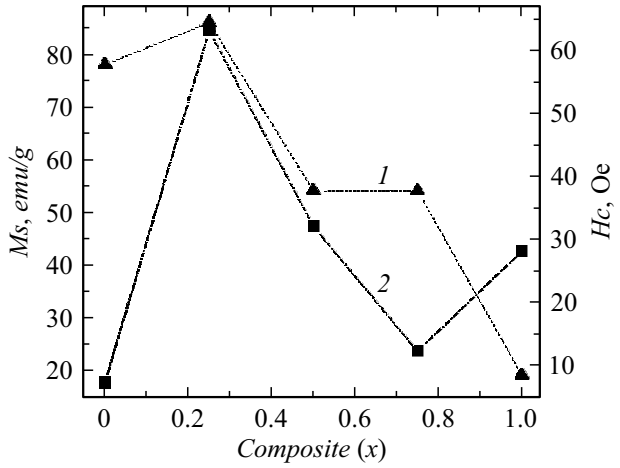

Figure 6. Saturation magnetization Ms (1) and coercivity Hc (2) of MNPs $Zn_xFe_{3-x}O_4$@PAA depending on Zn (x) content.

therein). The value of Ms-sample at Zn concentration $x = 0.25$ ($Zn_{0.25}Fe_{2.75}O_4$@PAA) reached 86 emu/g. Specially note that the Ms value of the synthesized MNPs ($Zn_{0.25}Fe_{2.75}O_4$@PAA) is much higher than the Ms value for Fe_3O_4 without doping, as well as for coated MNPs $Zn_xFe_{3-x}O_4$ [36], and is the highest among most inverse spinel ferrites alloyed with other metals (see [36] and references therein).

6. Mossbauer spectrometry of MNPs of spinel ferrites

Mossbauer spectroscopy makes it possible to uniquely identify iron oxides (hematite, magnetite, maghemite) and other iron-containing materials, as well as the actual percentage of these materials, which is impossible using X-ray diffraction analysis, as well as other methods. Therefore, the Mossbauer effect is widely used to study the phase composition, magnetic interactions, structural and magnetic properties of iron-containing materials [46], spinel ferrites [40–42], nanocomposites [48, 49], magnetic relaxation phenomena [50,51], as well as bimagnetic structures of the core–shell type [43–45].

The distinctive feature of magnetic particles is superparamagnetic relaxation, which occurs at such small sizes of particles, when thermal energy overcomes the energy of anisotropy and the orientation of the magnetization of the particle changes from one direction of the light axis to another [50,51]. Such feature substantially complicates the form of the Mossbauer spectra of (MS) MNPs, as can be seen in Fig. 7, *a* and Fig. 8, *a*. Therefore, to process the experimental spectra, we used a complex procedure of fitting and recovering from MS the probability functions of the distribution of effective magnetic fields $\{P(H_{\text{eff}})\}$ [29]. The process of such fitting includes: (1) a set of sextuplets whose relaxation times exceed the limit of the time window of the experiment (10^{-8} s), and therefore reveal blocked particles, (2) quadrupole doublets formed from superparamagnetic particles whose relaxation times are less than the value of the time window (10^{-8} s), and (3) Zeeman sextuplets with wide lines whose relaxation times are intermediate. Analysis of $P(H_{\text{eff}})$ curves makes it possible to establish the components of sextuplets and doublets, make their quality analysis, and draw conclusions about the belonging of these components to the corresponding iron oxides and positions of Fe ions in the crystal lattice [44,45,48,49].

6.1. Mossbauer studies of MNPs $Zn_xFe_{3-x}O_4$ $(0 \le x \le 1)$

Figure 7, *a* shows the experimental MS of MNPs $Zn_xFe_{3-x}O_4$ $(0 \le x \le 1)$ without PAA coating obtained at room temperature (300 K). Note that the experimental MS $Zn_xFe_{3-x}O_4$ (Fig. 7, *a*) are similar to those obtained, e. g. in [38,52–58] and reference therein. The dots in Fig. 7, *a* denote the experimental values, while the model components obtained using the program [29] are shown as solid lines. Restored from the experimental MS (Fig. 7, *a*) the probability function of the distribution of effective magnetic fields $(P(H_{\text{eff}}))$ are presented in Fig. 7, *b*. Using the positions on the rate scale of the absorption lines, we calculated the parameters of hyperfine interactions (HFI), namely, isomeric shifts (IS), quadrupole splittings (QS), effective magnetic fields (H_{eff}) given for MNPs $Zn_xFe_{3-x}O_4$ $(0 \le x \le 1)$ in Table 1. IS values are given relative to the metal foil of α-Fe.

The Mossbauer spectra of magnetite macrocrystals (not shown here) are a superposition of two partial Zeeman sextiplets corresponding to tetrahedral (Fe^{3+}) and octahedral (Fe^{3+} and Fe^{2+}) positions of iron atoms in the crystal lattice Fe_3O_4 [59]. The experimental spectra of MNPs (Fig. 7, *a* and 8, *a*) have a fundamentally different form. Mossbauer spectra of MNPs $Zn_xFe_{3-x}O_4$ at $x = 0$ (Fe_3O_4)

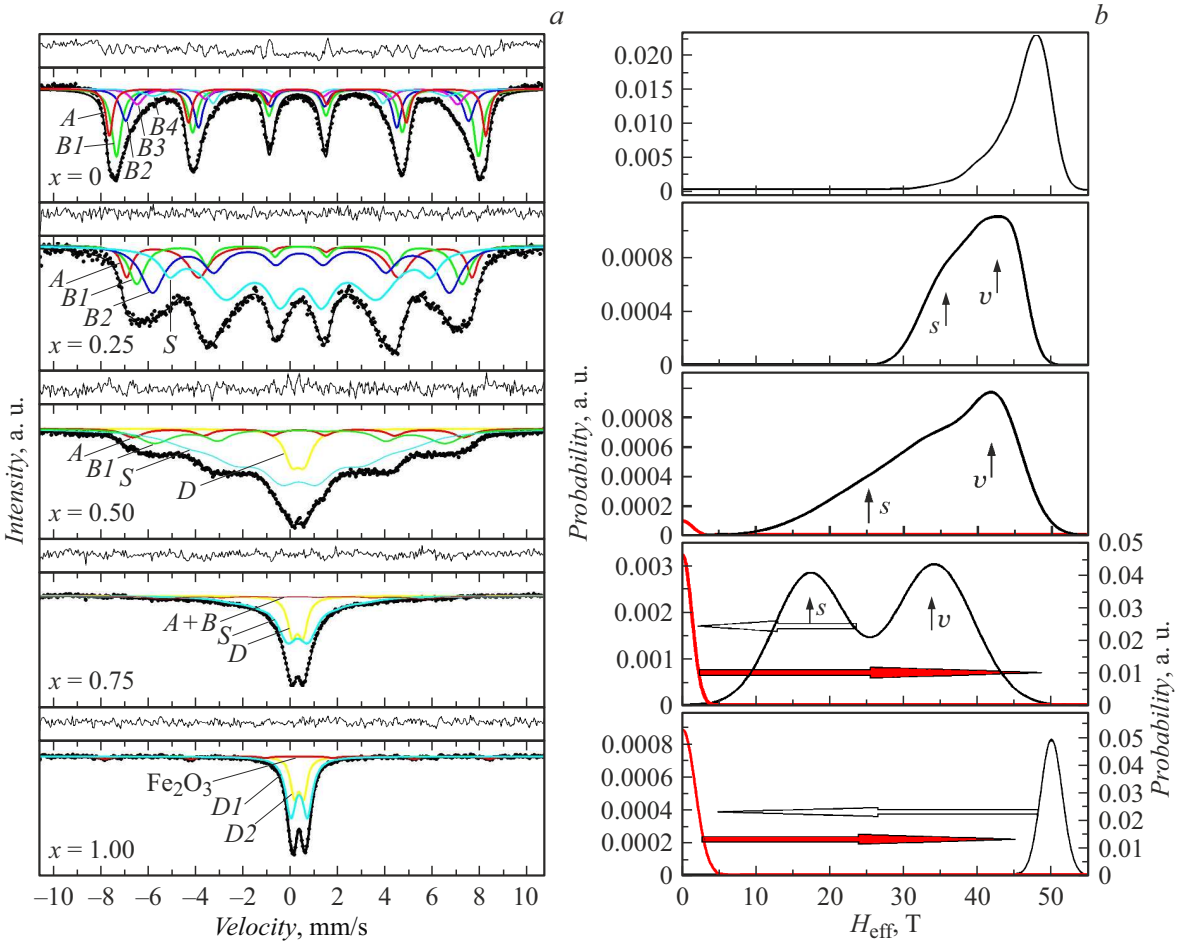

Figure 7. (*a*) — experimental MS at room temperature of MNPs $Zn_xFe_{3-x}O_4$ (for $x = 0$, 0.25, 0.5, 0.75 and 1.0) and their model representations. The sextiplets denoted as *A* refer to Fe ions in the *A*-sublattice; B_i (where i varies from 1 to 4) — to Fe ions in the *B*-sublattice; *D* — ions of Fe particles in the paramagnetic phase; *S* — Zeeman sextiplets of Fe ions in the surface layer of particles. *b* — $P(H_{\text{eff}})$ functions recovered from experimental MS of MNPs $Zn_xFe_{3-x}O_4$, using the program [29]. Here *S* are values of effective magnetic fields (H_{eff}) of iron ions occupying positions in the surface layer of MNPs, *V* are values of effective fields (H_{eff}) of iron ions located in the bulk of MNPs. The peak at $x = 1.0$ in the region H_{eff} 50 T refers to hematite.

consist of wide lines of Zeeman sextiplets. An increase in the amount of Zn ($x = 0.25$) leads to a decrease in intensity, a decrease in the amount of splitting and an increase in the widths of the Zeeman lines. The large widths of the Zeeman lines of the MS of $Zn_xFe_{3-x}O_4$ samples indicate the distribution of effective magnetic fields acting on the nuclei of Fe^{3+}, which, in turn, indicates the particle size distribution. With a further increase in the amount of zinc ($x = 0.5$), there is a gradual „collapse“ of Zeeman sextuplets and the appearance of doublet lines in the zero velocity region. At the $x = 0.75$ on the MS of MNPs $Zn_{0.75}Fe_{2.25}O_4$ the intensity of the lines of Zeeman sextuplets decreased significantly (Fig. 7, *a*), and the intensity of the doublet line increased significantly, and at $x = 1.0$ the Zeeman lines disappear and only the lines of the doublets are observed. When even a weak external magnetic field is applied, a significant transformation of the spectra occurs, which is characteristic of FM particles ([51,60–62] and references therein).

Functions $P(H_{\text{eff}})$ (Fig. 7, *b*) recovered from experimental MS of MNPs $Zn_xFe_{3-x}O_4$ (Fig. 7, *b*) differ from the functions for Fe_3O_4 macrocrystals (not shown here), where only two maxima are observed, which belong to iron ions in two nonequivalent positions. For MNPs $Zn_xFe_{3-x}O_4$ at Zn concentrations $x = 0.25$ on function $P(H_{\text{eff}})$ (Fig. 7, *b*) two maxima can be distinguished, one of which is at $H_{\text{eff}} \approx 43$ T, and the other at $H_{\text{eff}} \approx 36$ T denoted as *V* and *S* respectively. As the amount of Zn increases, the values of $P(H_{\text{eff}})$ decrease in the direction of H_{eff} decreasing. The amount of Zn increasing to $x = 0.5$ leads to an expansion of the H_{eff} decay region to ≈ 10 T with a simultaneous decreasing of H_{eff} value. This means that as the number of Zn ions increases in $Zn_xFe_{3-x}O_4$, the number of small particles gradually increases and the particle size distribution area increases.

At $x = 0.5$ in the region 0–5 T on the curve $P(H_{\text{eff}})$ a line appears, the intensity of which increases to a maximum with an increase in the content of Zn ions to $x = 1.0$. This

Table 1. The widths of the first and sixth lines (G) of Zeeman splitting, as well as the isomeric shifts (IS), quadrupole splitting (QS), effective magnetic fields ($H_{texteff}$) and subspectrum area (S) for iron ions at room temperature depending on ions Zn in $Zn_xFe_{3-x}O_4$ content

$Zn_xFe_{3-x}O_4$	Component	G, mm/s	IS, mm/s	QS, mm/s	H_{eff}, T	S, %
$x = 0$	A	0.462 ± 0.011	0.337 ± 0.002	0.003 ± 0.004	48.94 ± 0.02	31
	$B1$	0.547 ± 0.015	0.336 ± 0.002	0.003 ± 0.004	46.58 ± 0.03	35
	$B2$	0.481 ± 0.000	0.352 ± 0.005	0.016 ± 0.010	43.63 ± 0.06	15
	$B3$	0.548 ± 0.000	0.293 ± 0.011	0.162 ± 0.021	40.72 ± 0.11	9
	$B4$	1.115 ± 0.000	0.545 ± 0.026	0.078 ± 0.047	37.91 ± 0.23	11
$x = 0.25$	A	0.527 ± 0.129	0.313 ± 0.019	0.032 ± 0.036	45.19 ± 0.20	14
	$B1$	0.817 ± 0.310	0.371 ± 0.020	0.067 ± 0.043	42.55 ± 0.33	13
	$B2$	0.940 ± 0.390	0.368 ± 0.029	0.062 ± 0.051	38.81 ± 0.48	25
	S	1.167 ± 0.285	0.383 ± 0.024	0.040 ± 0.047	34.14 ± 0.53	48
$x = 0.5$	A	1.013 ± 0.000	0.305 ± 0.027	0.077 ± 0.054	43.09 ± 0.16	7
	$B1$	1.801 ± 0.184	0.462 ± 0.026	0.192 ± 0.054	37.18 ± 0.24	16
	S	2.519 ± 0.227	0.363 ± 0.014	0.074 ± 0.033	22.63 ± 0.45	72
	D	0.432 ± 0.036	0.343 ± 0.006	0.423 ± 0.013	–	5
$x = 0.75$	$A + B$	1.708 ± 0.000	0.242 ± 0.071	0.185 ± 0.133	34.00 ± 0.54	10
	S	1.600 ± 0.000	0.354 ± 0.039	0.005 ± 0.074	17.30 ± 0.60	67
	D	0.479 ± 0.025	0.344 ± 0.004	0.450 ± 0.010	–	24
$x = 1.0$	Fe_2O_3	0.489 ± 0.000	0.376 ± 0.028	0.230 ± 0.055	50.41 ± 0.23	7
	$D1$	0.364 ± 0.042	0.336 ± 0.003	0.392 ± 0.034	–	31
	$D2$	0.506 ± 0.010	0.344 ± 0.002	0.700 ± 0.041	–	63

line, corresponding to the doublet on the MS, indicates that at $x = 0.5$ in the MNPs $Zn_xFe_{3-x}O_4$, small particles are formed in the paramagnetic state, and the number of such particles increases when replaced with Zn ions from $x = 0.5$ to 1.0. Note that the doublet with similar parameters was observed for $Zn_xFe_{3-x}O_4$ in [55]. The second maximum at $x = 1.0$ in the region $H_{\text{eff}} \approx 50$ T refers to the Zeeman sextuplet (ZS), the analysis of the HFI parameters of which indicate its belonging to hematite.

The peak on the function $P(H_{\text{eff}})$, denoted as S, with an increase in the number of ions from $x = 0$ to 0.5 moves away from the V line towards smaller values H_{eff}. At $x = 0.75$ on the curve $P(H_{\text{eff}})$ two clearly resolved peaks are observed. It can be assumed that the peak V is formed by Fe ions located inside (in volume) of $Zn_xFe_{3-x}O_4$ particles, whereas peak S belongs to iron ions occupying positions in the surface layer of the MNPs. The peak S assignment to Fe ions located in the surface layer of the particles under study is based on the following. Calculations using the molecular orbital method showed that the contributions to H_{eff} from each of the indirect exchange bonds for the Fe^{3+} ion in the spinel structure for the octa- and tetrahedral positions are 8 and 12 kOe respectively [63,64]. In the nearest cationic environment of the $Fe^{3+}(A)$ ion, there are 12 iron ions in B-positions, and for the iron ion in the B-site — 6 iron ions in A- positions, the absence of half of the superexchange bonds should lead to a decrease in effective magnetic fields by several tens of kOe, which is consistent with the data of papers [45,49,65] and our experimental data.

Thus, at Zn concentrations between 0 and 0.75 MNPs $Zn_xFe_{3-x}O_4$ are core/shell particles in which the magnetically ordered core is surrounded by a shell where the superexchange interaction and therefore the effective magnetic fields are less than in the volume of the particle, as shown in [45,49,63,64]. Another possible explanation is the formation in the surface layer of particles of a beveled structure of magnetic moments relative to the orientation of moments in the volume of MNPs [66–68]. Features of the functions of (H_{eff}) (Fig. 7, b) reflect the complex magnetic structure of the studied MNPs $Zn_xFe_{3-x}O_4$, which cannot be explained only by the fact that when Zn ions are introduced, the distribution of ions surrounding iron ions changes.

Analysis of MS (Fig. 7, a) and functions $P(H_{\text{eff}})$ in Fig 7, b, showed that for a satisfactory description of MS of $Zn_xFe_{3-x}O_4$ ($0 \le x \le 1.0$) according to the criterion χ^2 it is necessary to use the superposition of several partial ZS and doublet. Therefore, to obtain quantitative information about the values of the parameters of hyperfine interactions, the experimental MS of MNPs $Zn_xFe_{3-x}O_4$ (Fig. 7, a) were processed using models individual for each concentration of Zn, differing in the number of partial sextuplets and doublets. The obtained HFI parameters are given in Table 1.

The change in hyperfine fields as a function of Zn concentration can be understood on the basis of theory of molecular and superexchange fields. According to Neel

theory, the contribution to the hyperfine magnetic field is due to the strongest exchange interactions of $A-B$, and the contributions due to the exchange interactions $A-A$ or $B-B$ are very small, and therefore they can be neglected. Ions Zn, being diamagnetic, do not participate directly in exchange interactions. The replacement of Fe^{3+} ions with Zn^{2+} weakens the superexchange interactions of $Fe_A^{3+}-O^{2-}-Fe_B^{3+}$, and therefore the hyperfine magnetic field is expected to decrease with increasing number of Zn ions. The MS also shows that as particle size decreases, hyperfine magnetic fields decrease and ZS line widhs increase. Fluctuation of magnetization vectors in the direction close to the direction of easy magnetization leads to the dependence of hyperfine fields on particle size [51,61].

On MS of magnetite macrocrystals, the Zeeman components belonging to the Fe^{2+} and Fe^{3+} ions are reliably identified by their IS, making $\sim 0.2-0.5$ mm/s for ions Fe^{3+} and $\sim 0.9-1.1$ mm/s for Fe^{2+} [55]. However, for the spinel ferrite MNPs the IS values of ions in the high-spin state Fe^{3+} are usually within the range of $0.3-0.6$ mm/s [69,70]. Large values of IS (from 0.9 to 1.1 mm/s) belong to iron ions in the low-spin state Fe^{2+}. As can be seen in Table 1, the IS values are within $0.3-0.5$ mm/s, indicating that in the MNPs $Zn_xFe_{3-x}O_4$ under study only Fe^{3+} ions are present. The IS values (Table 1) for different ZS differ little and, therefore, using IS it is impossible to identify whether the lines belong to nonequivalent positions of Fe ions. Therefore, the identification of the ZS is based on the conclusions of papers [71,72], indicating that in spinel ferrites MFe_2O_4 (M — metal ions) the hyperfine magnetic field of Fe ions at A- nodes is greater than in B- nodes. Therefore, in the MNPs $Zn_xFe_{3-x}O_4$ (Fig. 7, a) Zeeman component with a maximum value of H_{eff} represents the ions Fe^{3+} at position A. The remaining ZS (B_i, where i varies from 1 to 4) with smaller H_{eff} characterize Fe^{3+} ions at position B having different environments.

The average block temperature T_B in Mossbauer experiments is defined as the temperature at which half of magnetic moments of irom atoms is fixed in space during the measurement timeline, which on the MS is observed as Zeeman components (unblocked behavior), whereas magnetic moments for the other half of iron ions oscillate, giving a pure zero value H_{eff}, and on the MS are registered as a doublet lines (unblocked behavior) [73,74]. So, on MS of $Zn_xFe_{3-x}O_4$ at $0 \le x \le 0.25$, only the ZS lines are observed, and at $0.25 < x \le 0.75$ there are lines of doublets whose area is significantly less than the area of sextiplets indicating that the blocking temperature of these particles is below 300 K. In the case of the MNPs $ZnFe_2O_4$ ($x = 1.0$), the ZS area is much smaller than the area of the doublets, indicating that TB is significantly higher than room temperature. At temperatures below T_B each value of the hyperfine field relates to the volume of the particle [66], so function $P(H_{\text{eff}})$ can be considered as particles size distribution.

6.2. Mossbauer studies of MNPs $Zn_xFe_{3-x}O_4$@PAA ($0 \le x \le 1$)

The Mossbauer spectra of MNPs $Zn_xFe_{3-x}O_4$@PAA at room temperature are shown in Fig. 8, a. The distribution probabilities $P(H_{\text{eff}})$ recovered from the experimental MS, are shown in Fig. 8, b and the calculated HFI parameters in Table 2.

The Mossbauer spectra of MNPs $Zn_xFe_{3-x}O_4$@PAA (Fig. 8, a) differ significantly from spectra of uncoated MNPs $Zn_xFe_{3-x}O_4$ (Fig. 7, a). Thus, at $x = 0$, the linewidths of sextiplets are quite narrow, so they can be described by three ZSs belonging to iron ions occupying A, $B1$, and $B2$ positions of the crystal lattice. Substitution with Zn ions ($x = 0.25$ and $x = 0.5$) leads to a significant increase in the widths of the Zeeman lines due to the H_{eff} distribution, which, in turn, indicates an increase in the particles size distribution range. The convergence of the Zeman lines observed in this case means a decrease in H_{eff} and, accordingly, a decrease in the particle size. In the region of substitution by Zn ions from 0 to 0.25, only ZS lines are present on the MS; therefore, the blocking temperature (T_B) of these particles is higher than room temperature. At $x = 0.5$ against the background of the ZS, a clearly allowed doublet is observed, the intensity of which increases with an increase in Zn, and at $x = 1.0$ only the lines of the doublet remain. For Zn concentrations from $x = 0.25$ to 0.75, on the functions $P(H_{\text{eff}})$ one can distinguish maxima indicated in Fig. 8, b by arrows V and S; MS of MNPs $Zn_xFe_{3-x}O_4$@PAA at $x = 0.75$ is described by three ZS, one of which has clearly defined lines. The HFI parameters of this sextiplet indicate that it belongs to hematite, which agrees with XDP data. The line intensities on the MS of the second ZS at $x = 0.75$ (Fig. 8, a) are insignificant, and the value $H_{\text{eff}} \cong 42.5$ T corresponding on the distribution $P(H_{\text{eff}})$ to peak V, suggests that this sextiplet belongs to Fe ions located in the volume of MNPs $Zn_{0.75}Fe_{2.25}O_4$. The sextiplet corresponding on the function $P(H_{\text{eff}})$ to peak S at ~ 36 T refers to the iron ions located in the surface layer of the particles.

At $x = 1.0$, the Zeeman lines completely disappear and the MSs, as can be seen in Fig. 8, a, are described by doublets of iron ions in the paramagnetic phase and, according to IS, in the high-spin state (Fe^{3+}). The doublet with lower IS refers to iron ions in the tetrahedral A- position. The smaller isomeric shift for Fe ions in A-positions than in B-positions is formed due to the higher bond covalence of the Fe−O of A-positions.

Mossbauer studies of functionalized MNPs $Zn_xFe_{3-x}O_4$@PAA indicate that at substitution values from 0 to 0.75 these particles have a core/shell structure. In this case, the core is in a magnetically ordered state, while the shell is in a magnetically disordered phase. The reasons for the formation of core/shell structure were described in Sec. 6.1 and consist in a decrease in superexchange interactions in the surface layer of particle compared to interactions in the bulk. Therefore, the effective magnetic

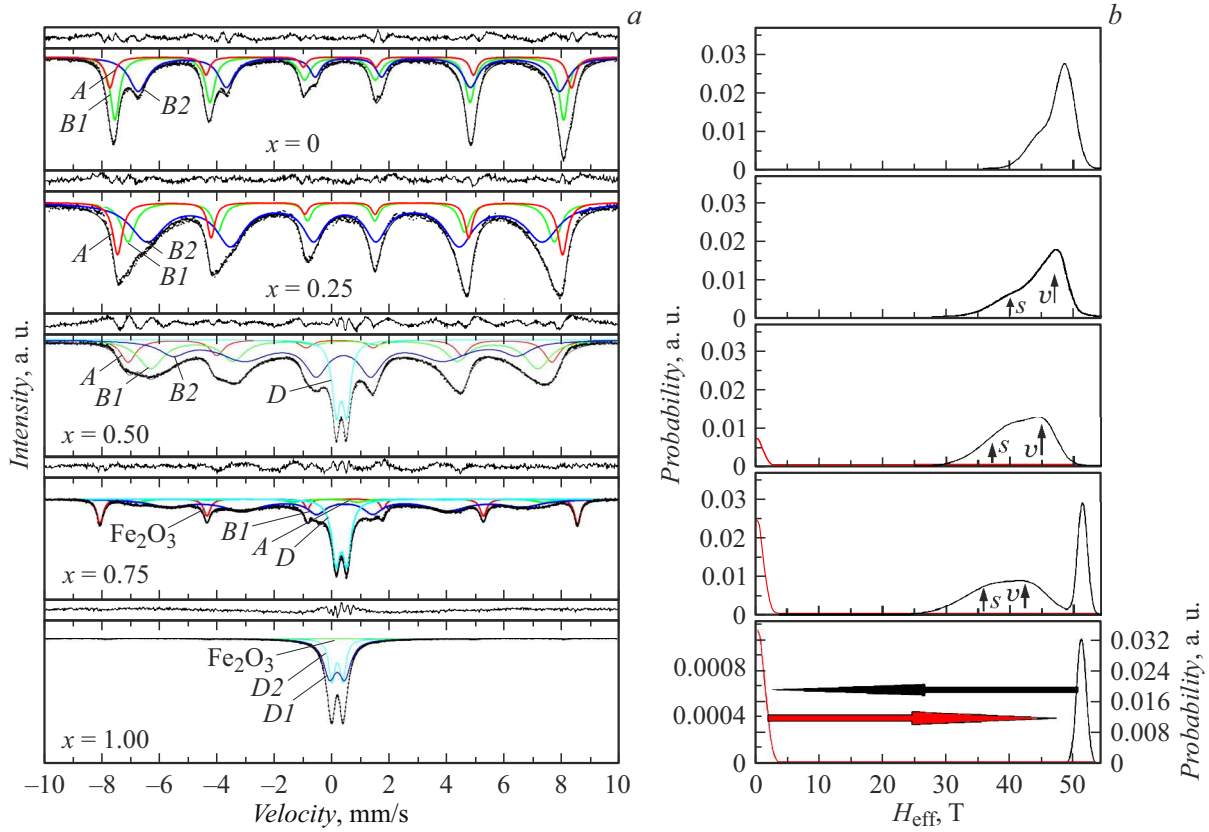

Figure 8. *a* — experimental MS at room temperature of MNPs $Zn_xFe_{3-x}O_4$@PAA (at $x = 0$, 0.25, 0.5, 0.75 and 1.0) and their model representations. The sextiplet for iron ions in the tetrahedral sublattice is denoted by the letter *A*, in the octahedral sublattices — *B1*, *B2* and *B3*, and the doublets determined by the particles of paramagnetic phase — *D*; *b* — $P(H_{\text{eff}})$ functions recovered from experimental MS of MNPs $Zn_xFe_{3-x}O_4$@PAA using program [29].

Table 2. The widths of the first and sixth lines (G) of Zeeman sextiplets, as well as the isomeric shifts (IS), quadrupole splitting (QS), effective magnetic fields (H_{eff}) and subspectrum area (S_q) for iron ions at room temperature of MNPs $Zn_xFe_{3-x}O_4$@PAA depending on number of ions Zn (x)

$Zn_xFe_{3-x}O_4$@PAA	Component	G, mm/s	IS, mm/s	QS, mm/s	H_{eff}, mm/s	S_q, %
0	*A*	0.357 ± 0.009	0.320 ± 0.002	0.029 ± 0.004	49.92 ± 0.02	15
	B1	0.381 ± 0.006	0.301 ± 0.001	0.025 ± 0.002	48.52 ± 0.01	42
	B2	0.787 ± 0.011	0.615 ± 0.002	0.013 ± 0.004	45.54 ± 0.02	43
0.25	*A*	0.405 ± 0.008	0.298 ± 0.001	0.005 ± 0.002	48.00 ± 0.02	17
	B1	0.572 ± 0.021	0.339 ± 0.002	0.003 ± 0.003	45.96 ± 0.03	20
	B2	1.386 ± 0.018	0.462 ± 0.002	0.007 ± 0.005	42.63 ± 0.04	63
0.5	*A*	0.640 ± 0.008	0.301 ± 0.001	0.016 ± 0.003	45.69 ± 0.01	15
	B1	1.041 ± 0.019	0.470 ± 0.001	0.034 ± 0.003	41.79 ± 0.02	28
	B2	1.130 ± 0.017	0.459 ± 0.002	0.049 ± 0.004	37.13 ± 0.05	45
	D	0.330 ± 0.001	0.356 ± 0.000	0.366 ± 0.001	–	12
0.75	Fe_2O_3	0.249 ± 0.003	0.377 ± 0.001	0.226 ± 0.002	51.50 ± 0.01	17
	A	0.802 ± 0.061	0.045 ± 0.011	0.480 ± 0.021	43.91 ± 0.10	7
	B1	1.610 ± 0.055	0.486 ± 0.005	0.018 ± 0.010	38.23 ± 0.06	52
	D	0.338 ± 0.002	0.356 ± 0.001	0.378 ± 0.001	–	26
1.0	Fe_2O_3	0.301 ± 0.000	0.385 ± 0.007	0.207 ± 0.014	51.25 ± 0.06	2
	D1	0.256 ± 0.006	0.352 ± 0.000	0.393 ± 0.001	–	36
	D2	0.517 ± 0.005	0.348 ± 0.000	0.541 ± 0.008	–	63

fields in the surface layer are smaller than the fields of iron ions located in the bulk of particles. Another reason may be that in the surface layer the magnetic moments form a certain angle with the moments in the MNP bulk, the so-called effect of the beveled state of the spin moments of iron ions located in the surface layer [66–68,74].

7. Size estimation of synthesized MNPs

In the literature, there are many papers related to the study of MS changes depending on the size of MNP [52–54,58,60,75,76], and in those papers the sizes of the studied particles were monitored by various methods. Comparison of experimental MS of $Zn_xFe_{3-x}O_4$ and $Zn_xFe_{3-x}O_4$@PAA particles with the published ones makes possible to estimate the sizes of the studied MNPs. For example, the papers [52–54,58,75,76] present the results of Mossbauer studies of MNPs with sizes from 3 to 98 nm. In [49] $Zn_xFe_{3-x}O_4$ MNPs with sizes (according to XDP data) ranging from 21 to 7 nm, and upon substitutions with Zn ions greater than $x = 0.2$ MS similar to those shown in Fig. 7, *a* were obtained at the same Zn content. With smaller numbers of Zn ions, the ZS of nonequivalent sublattices observed in the [52] are resolved, in contrast to the MSs shown in Fig. 7, *a*, on which the line resolution is absent, which means that the sizes the particles studied by us are smaller than 21 nm. Mossbauer spectroscopy of $Zn_xFe_{3-x}O_4$ particles with sizes from 15 to 117 nm shown that upon substitution $x = 0.5$ with size 15 nm on the MS of particles against the background of the ZS, a quadrupole doublet is observed, and with an increase in particle size, the intensity of the ZS lines increases [53]. In the same paper [53] for particles Fe_3O_4 ($x = 0$) with dimensions of 38 nm MS was obtained with split Zeeman lines of nonequivalent sublattices and the absence of a paramagnetic doublet. In [54] on MS of particles $Zn_xFe_{3-x}O_4$ with size from 40 nm (at $x = 0$) to 42 nm (at $x = 1.0$), doublet at $x = 1.0$ was observed even at the temperature of liquid nitrogen. This means that TB is below 77 K. Mossbauer spectra of particles $Zn_xFe_{3-x}O_4$ with size ~ 40 nm demonstrate the spectrum with splitted Zeeman lines for nonequivalent sublattices up to $x = 0.5$, and at $x = 1$, the spectrum consists of a quadrupole doublet [54]. On the MS of particles Fe_3O_4 with dimensions of 5.3 nm a wide singlet is observed, whereas in the case of particles of size 11 nm there is a ZS with a fairly good resolution of lines [75]. The Mossbauer spectra of MNPs $Zn_xFe_{4-x}O_{\{}0.01\}$ (at $0.8 \leq x \leq 3$) for sizes from 3 to 10 nm [58] are similar to those shown in Fig. 7, *a*.

Comparison of the obtained experimental MS with those published in the literature allows us to conclude that with increase in MNPs $Zn_xFe_{3-x}O_4$ doping with Zn ions from $x = 0$ up to 1.0, the particle sizes change smoothly from 15 to 5 nm. The Mossbauer data, indicating the decrease in particle size with increase in the number of Zn ions, are consistent with the results of SEM studies, but differ from the XDP data shown in Fig. 3.

Conclusion

The properties of $Zn_xFe_{3-x}O_4$ nanoparticles at $x = 0$, 0.25, 0.5, 0.75, 1.0 synthesized by the hydrothermal method and then functionalized (covered) by PAA $Zn_xFe_{3-x}O_4$@PAA were studied. The properties of MNPs depends on the number of doped Zn ions, as well as the effect of PAA coating (functionalization) on the properties of particles. The single-phase nature, the absence of impurities, and the superparamagnetic state of the synthesized particles are confirmed by XDP and MS data. Thus, no traces of iron-containing impurities and side phases were found on the MNP MS, and the X-ray diffraction patterns do not contain lines belonging to impurities and secondary phases.

Comparison of the obtained and published Mossbauer data showed that the size of the MNPs gradually decreases from 15 to 5 nm when replaced with Zn ions from $x = 0$ to 1.0. Mossbauer spectroscopy shows that both $Zn_xFe_{3-x}O_4$ particles and $Zn_xFe_{3-x}O_4$@PAA have a core/shell structure, in which the core is the magnetically ordered central region of the particles, and the shell is the magnetically disordered surface layer. The MS results indicate that the PAA coating leads to the particles isolation from each other. So, decrease or elimination of interactions between particles, decrease in the blocking temperature, decrease in the thickness of the paramagnetic shell and, due to this, increase in the diameter of the magnetically ordered core because of decreasing the thickness of the paramagnetic shell. Mossbauer studies revealed a new understanding of the magnetic structure of the particles under study, the effect of surface coating on the MNP properties, confirmed by X-ray diffraction and magnetic measurements.

In conclusion, it was shown that MNPs $Zn_xFe_{3-x}O_4$ were synthesized by a simple hydrothermal method. PAA functionalization created MNPs that combine multifunctionality and superparamagnetism, as well as biological compatibility, which makes them promising for various applications, including biomedicine, in particular, drug delivery, magnetic hyperthermia, and image contrast enhancement.

Funding

N. Dogan and A. Bingolbali express their gratitude for the financial support of the Scientific and Technological Research Council of Turkey (TUBITAK grants: № 115E776 and № 115E777).

Conflict of interest

The authors declare that they have no conflict of interest.

References

[1] S.A. Novopashin, M.A. Serebryakova, S.Ya. Khmel. Teplofizika i aeromekhanika, **22**, (411), (2015) (in Russian).

[2] *Low Viscosity Magnetic Fluid Obtained by the Colloidal Suspension of Magnetic Particles* (pat. 3215572A USA. Papell S.S.; Applic. 09.10.1963; Publ. 02.11.1965)

[3] R.E. Rosensweig, R. Kaiser. *NTIS Rep. No. NASW-1219; NASA Rep. NASACR-91684. NASA Office of Advanced Research and Technology* (Washington, DC, 1967), 238 p.

[4] M.A.A. Kerroum, C. Iacovita, W. Baaziz, D. Ihiawakrim, G. Rogez, M. Benaissa, C.M. Lucaciu, O. Ersen. Int. J. Mol. Sci., **21**, 7775 (2020). DOI: 10.3390/ijms21207775

[5] J.A. Ramos-Guivar, E.O. Lopez, J.-M. Greneche, F.J. Litterst, E.C. Passamani. Appl. Surf. Sci., **538**, 148021 (2021). DOI: 10.1016/j.jmmm.2022.169241

[6] W. Wang, J.V.I. Timonen, A. Carlson, D.-M. Drotlef, C.T. Zhang, S. Kolle, A. Grinthal, T.-S. Wong, B. Hatton, S.H. Kang, S. Kennedy, J. Chi, R.T. Blough, M. Sitti, L. Mahadevan. J. Aizenberg. Nature, **559**, 77 (2018). DOI: 10.1038/s41586-018-0250-8

[7] M. Abdolrahimi, M. Vasilakaki, S. Slimani, N. Ntallis, G. Varvaro, S. Laureti, C. Meneghini, K.N. Trohidou, D. Fiorani, D. Peddis. Nanomaterials, **11**, 1787 (2021). DOI: 10.3390/nano11071787

[8] E.M. Materon, C.M. Miyazaki, O. Carr, N. Joshi, P.H.S. Picciani, C.J. Dalmaschio, F. Davis, F.M. Shimizu. Appl. Surf. Sci. Adv., **6**, 100163 (2021). DOI: 10.3390/bios12080554

[9] M.G.M. Schneider, M.J. Martín, J. Otarola, E. Vakarelska, V. Simeonov, V. Lassalle, M. Nedyalkova. Pharmaceutics, **14**, 204 (2022). DOI: 10.3390/pharmaceutics14010204

[10] I.M. Obaidat, V. Narayanaswamy, S. Alaabed, S. Sambasivam, C.V.V.M. Gopi. Magnetochemistry, **5**, 67 (2019). DOI: 10.3390/magnetochemistry5040067

[11] J. Majeed, L. Pradhan, R.S. Ningthoujam, R.K. Vatsa, D. Bahadur, A.K. Tyagi. Colloids Surf. B, **122**, 396 (2014). DOI: 10.1016/j.colsurfb.2014.07.019

[12] M. Nedyalkova, B. Donkova, J. Romanova, G. Tzvetkov, S. Madurga, V. Simeonov. Adv. Colloid Interface Sci., **249**, 192 (2017). DOI: 10.1016/j.cis.2017.05.003

[13] *Size Effects in Nanostructures: Basics and Applications*, ed. by V. Kuncser, L. Miu (Springer-Verlag, Berlin-Heidelberg, 2014)

[14] V. Šepelák. Ann. Chim. Sci. Mat., **27**, 61 (2002). DOI: 10.1016/S0151-9107(02)90015-2

[15] J. Bennet, R. Tholkappiyan, K. Vishista, N.V. Jaya, F. Hamed. Appl. Surf. Sci., **383**, 113 (2016). DOI: 10.1016/j.apsusc.2016.04.177

[16] T. Vigneswari, P. Rajib. J. Mol. Struct., **424**, 267 (2017). DOI: 10.1016/j.molstruc.2016.07.116

[17] F. Ozel, O. Karaagac, E. Tokay, F. Kockar, H. Kockar. J. Magn. Magn. Mater., **474**, 654 (2019). DOI: 10.1016/j.jmmm.2018.11.025

[18] H. Mahajan, S.K. Godara, A.K. Srivastava. J. Alloys Compd., **896**, 162966 (2021). DOI: 10.1016/j.jallcom.2021.162966

[19] E.A. Périgo, G. Hemery, O. Sandre, D. Ortega, E. Garaio, F. Plazaola, F.J. Teran. Appl. Phys. Rev., **2**, 041302 (2015). DOI: 10.1063/1.4935688

[20] *Iron Oxide Nanoparticles for Biomedical Applications: Synthesis, Functionalization and Application. A volume in Metal Oxides*, ed. by M. Mahmoudi, S. Laurent (Elsevier, 2018)

[21] P.D. Shima, J. Philip, B. Raj. J. Phys. Chem. C, **114**, 18825 (2010). DOI: 10.1021/jp107447q

[22] V. Kuncser, O. Crisan, G. Schinteie, F. Tolea, P. Palade, M. Valeanu, G. Filoti. *Modern Trends in Nanoscience* (Editura Academiei Romane, Bucharest, 2013), v. 197.

[23] M.A. Daniele, M.L. Shaughnessy, R. Roeder, A. Childress, Y.P. Bandera, S. Foulger. ACS Nano, **7**, 203 (2012). DOI: 10.1021/nn3037368

[24] C. Liu, P. Huang. Soil Sci. Soc. Am. J., **63**, 65 (1999). DOI: 10.2136/sssaj1999.03615995006300010011x

[25] A. Jedlovszky-Hajd, F.B. Bombelli, M.P. Monopoli, E. Tombacz, K.A. Dawson. Langmuir, **28**, 14983 (2012). DOI: 10.1021/la302446h

[26] M. Nandy, B.B. Lahiri, C.H. Yadhukrishna, J. Philip. J. Mol. Liq., **336**, 116332 (2021). DOI: 10.1016/j.molliq.2021.116332

[27] T.J. Daou, G. Pourroy, S. Begin-Colin, J.M. Greneche, C. Ulhaq-Bouillet, P. Legar, P. Bernhardt, C. Leuvrey, G. Rogez. Chem. Mater., **18**, 4399 (2006). DOI: 10.1021/cm060805r

[28] S. Xuan, L. Hao, W. Jiang, X. Gong, Y. Hu, Z. Chen. J. Magn. Magn. Mater., **308**, 210 (2007). DOI: 10.1016/j.jmmm.2006.05.017

[29] V.G. Semenov, V.V. Panchuk. Private message.

[30] K. Nakamoto. *Infrared and Raman Spectra of Inorganic and Coordination Compounds. Part B.* (Wiley, N.Y., 2009), p. 424.

[31] X. Wu, Z. Ding, W. Wang, N. Song, S. Khaimanov, N. Tsidaeva. Powder Technol., **295**, 59 (2016). DOI: 10.1016/j.powtec.2016.03.033

[32] K. Raja, S. Verma, S. Karmakar, S. Kar, S.J. Das, K.S. Bartwal. Cryst. Res. Technol., **46**, 497 (2011). DOI: 10.1002/crat.201100105

[33] B.D. Cullity. *Elements of X-ray Diffraction* (Addison Wesley Publishing Company, USA, 1978)

[34] Y. Tan, Z. Zhuang, Q. Peng, Y. Li. Chem. Mater., **20**, 5029 (2008). DOI: 10.1021/cm801082p

[35] M. Abareshi, E.K. Goharshadi, S. Mojtaba Zebarjad, H. Khandan Fadafan, A. Youssefi. J. Magn. Magn. Mater., **322**, 3895 (2010). DOI: 10.1016/j.jmmm.2010.08.016

[36] J. Liu, Y. Bin, M. Matsuo. J. Phys. Chem. C, **116**, 134 (2012). DOI: 10.1021/jp207354s

[37] K. Praveena, K. Sadhana, H.S. Virk. Solid State Phenom., **232**, 45 (2015). DOI: 10.4028/www.scientific.net/SSP.232.45

[38] M. Srivastava, S.K. Alla, S.S. Meena, N. Gupta, R.K. Mandal, N.K. Prasad. New J. Chem., **42**, 07144 (2018). DOI: 10.1039/C8NJ00547H

[39] M. Abbas, B.P. Rao, S.M. Naga, M. Takahashi, C. Kim. Ceram. Int., **39**, 7605 (2013). DOI: 10.1016/j.ceramint.2013.03.01

[40] M.S. Angotzi, A. Musinu, V. Mameli, A. Ardu, C. Cara, D. Niznansky, H.L. Xin, C. Cannas. ACS Nano, **11**, 7889 (2017). DOI: 10.1021/acsnano.7b02349

[41] *Mossbauer Spectroscopy Applied to Magnetism and Materials Science*, ed. by G.J. Long, F. Grandjean (Springer Science+Business Media, NY., 1993), v. 1, 479 p.

[42] B. Fultz. *Mössbauer Spectrometry. Characterization of Materials* (John Wiley & Sons, Inc., Hoboken, N.J., 2011)

[43] E. Umut, M. Coşkun, H. Güngüneş, V. Dupuis, A.S. Kamzin. J. Supercond. Nov. Magn., **34**, 913 (2021). DOI: 10.1007/s10948-020-05800-y

[44] A.S. Kamzin, I.M. Obaidat, A.A. Valliulin, V.G. Semenov, I.A. Al-Omari. FTT, **62**, 1715 (2020) (in Russian). DOI: 10.21883/FTT.2020.10.49928.056
[45] A.S. Kamzin, I.M. Obaidat, A.A. Valliulin, V.G. Semenov, I.A. Al-Omari. FTT, **62**, 1919 (2020) (in Russian). DOI: 10.21883/FTT.2020.11.50071.062
[46] *Magnetic Properties of Fine Particles*, ed. by J.L. Dormann, D. Fiorani (Elsevier, 2012), 430 p.
[47] E.C. Stoner, E. Wohlfarth. Phil. Tr. Roy. Soc. Lond. Ser. A, **240**, 599 (1948). DOI: 10.1098/rsta.1948.0007
[48] A.S. Kamzin, I.M. Obaidat, V.S. Kozlov, E.V. Voronina, V. Narayanaswamy, I.A. Al-Omari. FTT, **63**, 807 (2021) (in Russian). DOI: 10.21883/FTT.2021.06.50944.004
[49] A.S. Kamzin, I.M. Obaidat, V.S. Kozlov, E.V. Voronina, V. Narayanaswamy, I.A. Al-Omari. FTT, **63**, 900 (2021) (in Russian). DOI: 10.21883/FTT.2021.07.51040.039
[50] R. Gabbasov, M. Polikarpov, V. Cherepanov, M. Chuev, I. Mischenko, A. Lomov, A. Wang, V. Panchenko. J. Magn. Magn. Mater., **380**, 111 (2015). DOI: 10.1016/j.jmmm.2014.11.032
[51] M.A. Chuev. Pisma v ZhETF, **98**, 523 (2013). (in Russian) [M.A. Chuev, JETP Lett., **98**, 465 (2013). DOI: 10.7868/S0370274X1320006X]
[52] J.M. Byrne, V.S. Coker, E. Cespedes, P.L. Wincott, D.J. Vaughan, R.A.D. Pattrick, G. van der Laan, E. Arenholz, F. Tuna, M. Bencsik, J.R. Lloyd, N.D. Telling. Adv. Funct. Mater., **24**, 2518 (2014). DOI: 10.1002/adfm.201303230
[53] P.M. Zelis, G.A. Pasquevich, S.J. Stewart, M.B.F. Van Raap, J. Aphesteguy, I.J. Bruvera, C. Laborde, B. Pianciola, S. Jacobo, F.H. Sanchez. J. Phys. D. Appl. Phys., **46**, 125006 (2013). DOI: 10.1088/0022-3727/46/12/125006.
[54] S.W. da Silva, F. Nakagomi, M.S. Silva, A. Franco Jr., V.K. Garg, A.C. Oliveira, P.C. Morais. J. Nanopart. Res., **14**, 798 (2012). DOI: 10.1007/s11051-012-0798-4
[55] S.B. Singh, Ch. Srinivas, B.V. Tirupanyam, C.L. Prajapat, M.R. Singh, S.S. Meena, P. Bhatt, S.M. Yusuf, D.L. Sastry. Ceram. Intern., **42**, 19188 (2016). DOI: 10.1016/j.ceramint.2016.09.081
[56] A.G. Roca, J.F. Marco, M. del P. Morales, C.J. Serna. J. Phys. Chem. C, **111**, 18577 (2007). DOI: 10.1021/jp075133m
[57] E.S. Vasil'eva, O.V. Tolochko, V.G. Semenov, V.S. Volodin, D. Kim. Tech. Phys. Lett., **33**, 40 (2007). DOI: 10.1134/S1063785007010117
[58] C.E. Johnson, J.A. Johnson, H.Y. Hah, M. Cole, S. Gray, V. Kolesnichenko, P. Kucheryavy, G. Goloverda. Hyperfine Interact., **237**, 27 (2016). DOI: 10.1007/s10751-016-1277-6
[59] E.R. Bauminger, S.G. Cohen, A. Marinov, S. Ofer, E. Segal. Phys. Rev., **122**, 1447 (1961). DOI: 10.1103/PhysRev.122.1447
[60] M.A. Chuev. Dokl. Phys., **56**, 318 (2011). DOI: 10.1134/S1028335811060097
[61] M.A. Chuev. J. Phys. Cond. Matter. **20**, 505201 (2008). DOI: 10.1088/0953-8984/20/50/505201
[62] M.A. Chuev, JETP, **114**, 609 (2012). DOI: 10.1134/S1063776112020185
[63] G.A. Sawatzky, C. Boekema, F. van der Woude. *Proc. Int. Conf. on the Appl. of the Mössbauer Effect* (Dresden, Germany, 1971), p. 238.
[64] F. van der Woude, G.A. Sawatzky. Phys. Rev. B, **4**, 3159 (1971). DOI: 10.1103/PhysRevB.4.3159
[65] I.N. Zakharova, M.A. Shipilin, V.P. Alekseev, A.M. Shipilin. Tech. Phys. Lett., **38**, 55 (2012).
[66] S. Morup, J.A. Dumesic, H. Topsee. In: *Applications of Mossbauer Spectroscopy*, ed. by R.L. Cohen (Academic Press, N. Y., 1980), v. II, p. 1.
[67] S. Mørup, E. Brok, C. Frandsen. J. Nanomater., 720629 (2013). DOI: 10.1155/2013/720629
[68] A.S. Kamzin. J. Experim. Theoret. Phys. **89**, 890 (1999).
[69] C.N. Chinnasamy, A. Narayanasamy, N. Ponpandian, K. Chattopadhyay, H. Guerault, J.-M. Greneche. J. Phys. Cond. Matter., **12**, 7795 (2000). DOI: 10.1088/0953-8984/12/35/314
[70] A.S. Kamzin, I.M. Obaidat, V.G. Semenov, V. Narayanaswamy, I.A. Al-Omari, B. Issa, I.V. Buryanenko. FTT, **64**, 712 (2022) (in Russian). DOI: 10.21883/FTT.2022.06.52406.298
[71] G.A. Sawatzky, F. Van der Woude, A.H. Morrish. J. Appl. Phys., **39**, 1204 (1968). DOI: 10.1063/1.1656224
[72] G.A. Sawatzky, F. Van der Woude, A.H. Morrish. Phys. Rev., **187**, 747 (1969). DOI: 10.1103/PhysRev.187.747
[73] E. Lima, A.L. Brandl, A.D. Arelaro, G.F. Goya. J. Appl. Phys., **99**, 083908 (2006). DOI: 10.1063/1.2191471
[74] J.M.D. Coey. Phys. Rev. Lett., **27**, 1140 (1971). DOI: 10.1103/PhysRevLett.27.1140
[75] S. Ferrari, J.C. Aphesteguy, F.D. Saccone. IEEE Tr. MAG, **51**, 2900206 (2015). DOI: 10.1109/TMAG.2014.2377132
[76] P. Masina, T. Moyo, H.M.I. Abdallah. J. Magn. Magn. Mater., **381**, 41 (2015). DOI: 10.1016/j.jmmm.2014.12.053